The rational synthesis of tetranuclear heterometallic butterfly clusters: reactions of $[M_2(CO)_6(\mu\text{-pyS})_2]$ (M = Re, Mn) with group VIII metal carbonyls†

Shishir Ghosh,[a] Kamrun N. Khanam,[a] G. M. Golzar Hossain,[b] Daniel T. Haworth,[c] Sergey V. Lindeman,[c] Graeme Hogarth*[d] and Shariff E. Kabir*[a]

Received (in Victoria, Australia) 1st October 2009, Accepted 17th February 2010
DOI: 10.1039/b9nj00526a

Heating $[Os_3(CO)_{10}(NCMe)_2]$ with $[M_2(CO)_6(\mu\text{-pyS})_2]$ (M = Re, Mn) (**1–2**) in benzene affords tetranuclear mixed-metal butterfly clusters $[MOs_3(CO)_{13}(\mu_3\text{-pyS})]$ (**3–4**). Similar reactions with $Ru_3(CO)_{12}$ give $[MRu_3(CO)_{13}(\mu_3\text{-pyS})]$ (**5–6**); however, when the latter is carried out in toluene the tetraruthenium sulfido cluster $[Ru_4(CO)_{12}(\mu\text{-py})_2(\mu_4\text{-S})]$ (**7**) is the major product. Treatment of $Fe_3(CO)_{12}$ with **1** in refluxing toluene affords the mixed-metal sulfido cluster, $[Fe_2Re_2(CO)_{13}(\mu\text{-py})(\mu\text{-pyS})(\mu_4\text{-S})]$ (**8**), while a similar reaction with **2** furnishes the tetrairon cluster $[Fe_4(CO)_{12}(\mu\text{-py})_2(\mu_4\text{-S})]$ (**9**). Addition of PPh_3 to **3** in the presence of Me_3NO affords both the mono- and bis(phosphine)-substituted products $[ReOs_3(CO)_{12}(PPh_3)(\mu_3\text{-pyS})]$ (**10**) and $[ReOs_3(CO)_{11}(PPh_3)_2(\mu_3\text{-pyS})]$ (**11**), respectively. All new complexes have been characterized by a combination of spectroscopic data and single-crystal X-ray diffraction studies.

Introduction

Recently, considerable attention has been devoted to the chemistry of heterometallic complexes, being primarily aimed at understanding cooperative effects originating when two different metal centers are in close proximity, which in turn may result in unique catalytic properties.[1–12] A key limitation in such studies is often the availability of efficient and high-yielding routes to the synthesis of the desired mixed-metal clusters. Consequently, few isostructural series are known whereby the precise role of each different metal type may be fully assessed.[13,14]

Studies of metal pyridine-2-thiolate complexes are stimulated by their structural diversity,[15,16] important biological roles,[17] and potential applications as precursors for metal-sulfide materials.[18] In 1988 Deeming *et al*. reported the high-yielding formation of $[Re_2(CO)_6(\mu\text{-pyS})_2]$ (**1**) from the reaction of $Re_2(CO)_{10}$ and pyridine-2-thiol (pySH).[19] Importantly, they found that slow scrambling of **1** with the 6-methylsubstituted analogue $[Re_2(CO)_6(\mu\text{-MepyS})_2]$ at room temperature gave an equilibrium involving $[Re_2(CO)_6(\mu\text{-pyS})(\mu\text{-MepyS})]$ and suggested that the scrambling process occurred *via* the 16-electron mononuclear species $[Re(CO)_3(pyS)]$ or a related solvent-stabilized 18-electron species. Believing that such transient mononuclear species might be precursors to heterometallic complexes, they treated **1** with $Ru_3(CO)_{12}$ in refluxing xylene in order to generate $[ReRu(CO)_x(pyS)]$ (x = 7 or 8). Instead, however, they obtained a series of tetranuclear compounds containing $ReRu_3$, Re_2Ru_2 and Re_3Ru cores linked by μ_4-sulfido and μ-2-pyridyl ligands.[20]

Recently, using the lability of the M–S bond in the 2-mercapto-1-methylimidazolate analogue of **1**, *i.e.* in $[Re_2(CO)_6(\mu\text{-}SN_2C_4H_5)_2]$ and its manganese analogue $[Mn_2(CO)_6(\mu\text{-}SN_2C_4H_5)_2]$, we have demonstrated the synthesis of two isostructural series at moderate temperatures (Scheme 1). Thus, the mixed-metal trinuclear clusters, $[MMn_2(CO)_8(\mu\text{-}CO)_2(\mu_3\text{-}SN_2C_4H_5)_2]$ (M = W, Mo, Cr), are obtained from the reactions between $[Mn_2(CO)_6(\mu\text{-}SN_2C_4H_5)_2]$ and $[M(CO)_3(NCMe)_3]$ (M = Cr, Mo, W) in THF. They consist of an open cluster of two manganese atoms and a third metal atom, M (M = W, Mo, Cr), linked by two M–Mn bonds, two triply-bridging 2-mercapto-1-methylimidazolate ligands and two asymmetrically bound μ-CO ligands.[21] On the other hand, tetranuclear mixed-metal clusters, $[M'_3M(CO)_{13}(\mu_3\text{-}SN_2C_4H_5)]$ (M′ = Os, Ru; M = Re, Mn), are formed from the reactions between $[M'_3(CO)_{10}L_2]$ (L = MeCN, CO) and $[M_2(CO)_6(\mu\text{-}SN_2C_4H_5)_2]$ (M = Re, Mn), consisting of a butterfly skeleton of four metal atoms with the unique metal atom occupying a wingtip position.[22] These successes promoted us to investigate the feasibility of using **1** in the synthesis of group 7/8 mixed-metal butterfly clusters at moderate temperature in order to extend the isostructural series of 2-mercapto-1-methylimidazole towards pyridine-2-thiol. Herein we describe the successful development of this strategy with the synthesis of a series of mixed-metal clusters $[M'_3M(CO)_{13}(\mu_3\text{-pyS})]$ (M = Os, Ru; M′ = Re, Mn) in good yields and we also present a preliminary study on the reactivity of one of these. We also show, however, that this strategy cannot be extended towards iron-containing clusters, since competing metal–metal and carbon–sulfur bond

[a] *Department of Chemistry, Jahangirnagar University, Savar, Dhaka 1342, Bangladesh*
[b] *Department of Chemistry, University of Dhaka, Dhaka 1000, Bangladesh*
[c] *Department of Chemistry, Marquette University, P.O. Box 1881, Milwaukee, Wisconsin 53201-1881, USA*
[d] *Department of Chemistry, University College London, 20 Gordon Street, London, WC1H 0AJ, UK*

† Electronic supplementary information (ESI) available: Crystal structure data. CCDC reference numbers 748787, 748072, 748073, 748074, 748075, 748076, 748077 and 721479. For crystallographic data in CIF or other electronic format see DOI: 10.1039/b9nj00526a

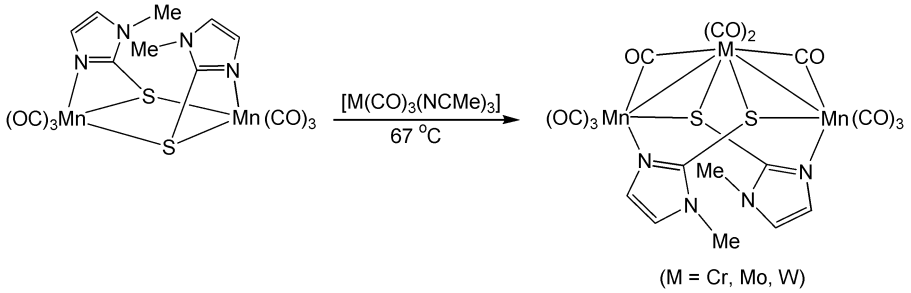

Scheme 1

scission processes compete to afford sulfido-bridged clusters instead of the desired products.

Results and discussion

(a) Synthesis of pyridine-2-thiolate capped mixed-metal butterfly clusters

Treatment of $[Os_3(CO)_{10}(NCMe)_2]$ with $[Re_2(CO)_6(\mu\text{-pyS})_2]$ (**1**) and $[Mn_2(CO)_6(\mu\text{-pyS})_2]$ (**2**) at 80 °C in benzene for 2 h afforded $[ReOs_3(CO)_{13}(\mu_3\text{-pyS})]$ (**3**) and $[MnOs_3(CO)_{13}(\mu_3\text{-pyS})]$ (**4**) as red, air-stable solids in 71 and 74% yields, respectively (Scheme 2). The analogous mixed Re–Ru and Mn–Ru clusters $[ReRu_3(CO)_{13}(\mu_3\text{-pyS})]$ (**5**) and $[MnRu_3(CO)_{13}(\mu_3\text{-pyS})]$ (**6**) were obtained in 42 and 38% yields, from similar reactions with $Ru_3(CO)_{12}$ (Scheme 2). All have been fully characterized by a combination of analytical and spectroscopic data together with single-crystal X-ray diffraction studies.

The ^{1}H NMR spectra of **3–6** display only aromatic resonances, each consisting of two doublets and two triplets (each integrating to 1H) which are attributed to the four ring hydrogen atoms of the pyridine-2-thiolato ligand. FAB mass spectra (+ve) of all four show a parent molecular ion (*m*/*z* 1232 for **3**, 1100 for **4**, 963 for **5** and 832 for **6**) together with ions due to sequential loss of thirteen carbonyl groups. Single-crystal structures have been carried out for **3**, **4** and **6**, the results of which are summarized in Fig. 1, Fig. 2 and Fig. 3. The overall structural features of these clusters are very similar. All contain four metal atoms which form a butterfly skeleton with the unique metal atom, M (M = Re, Mn), in a wingtip position. The pyridine-2-thiolato ligand is facially located on the convex side of the butterfly and simultaneously caps three metal atoms. Thus, it bridges the hinge metal atoms through the exocyclic sulfur atom, and coordinates to the group 7 metal atom through the ring nitrogen. The fold angle of the butterfly varies only slightly between the clusters; 156.7° in **3**, 157.8° in **4** and 158.0° in **6**. The distribution and coordination mode of the carbonyl ligands in all are similar and the gross structural features are very similar to the corresponding 2-mercapto-1-methylimidazole analogues, $[M_3M'(CO)_{13}(\mu_3\text{-}SN_2C_4H_5)]$ (M = Os, Ru; M′ = Re, Mn).[22]

When the reaction of $Ru_3(CO)_{12}$ with **2** was carried out at 110 °C in toluene (25 min), the tetraruthenium cluster $[Ru_4(CO)_{12}(\mu\text{-py})_2(\mu_4\text{-S})]$ (**7**) was isolated as the major product together with smaller amounts of **6** (Scheme 3). The FAB mass spectrum of **7** exhibits a parent molecular ion at *m*/*z* 928 and fragmentation ions due to successive loss of twelve carbonyl groups. The ^{1}H NMR spectrum shows four equally intense resonances in the aromatic region: two doublets at δ 7.81 (J = 6.8 Hz) and 7.57 (J = 6.8 Hz) and two triplets at δ 7.02 (J = 6.8 Hz) and 6.83 (J = 6.8 Hz) consistent with the proposed structure. However, the precise core geometry

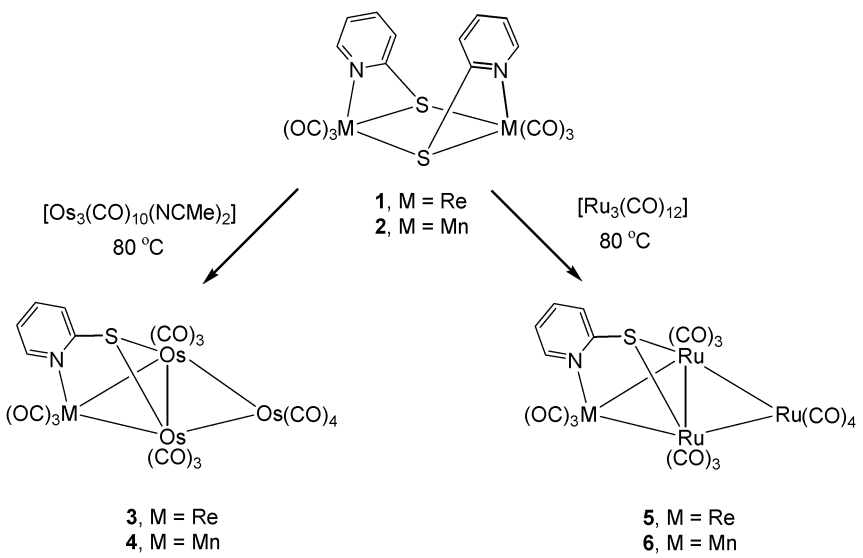

Scheme 2

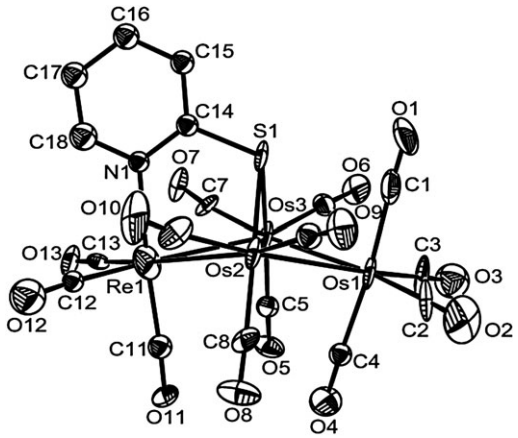

Fig. 1 ORTEP diagram of the molecular structure of $[Os_3Re(CO)_{13}(\mu_3\text{-pyS})]$ (**3**), showing 70% probability thermal ellipsoids. Ring hydrogen atoms are omitted for clarity. Selected interatomic distances (Å) and angles (°): Os(1)–Os(2) 2.8524(7), Os(1)–Os(3) 2.8549(7), Os(2)–Os(3) 2.7827(7), Os(2)–Re(3) 2.8842(7), Os(3)–Re(3) 2.9461(7), Os(2)–S(1) 2.405(3), Os(3)–S(1) 2.400(3), Re(3)–N(1) 2.244(9), C(14)–S(1) 1.774(12), Os(2)–Os(1)–Os(3) 58.363(15), Os(3)–Os(2)–Re(3) 62.619(18), Os(1)–Os(2)–Re(3) 119.238(19), Os(1)–Os(3)–Re(3) 117.09(2), Os(3)–Os(2)–Os(1) 60.865(16), Os(2)–Os(3)–Re(3) 60.376(17), Os(2)–Re(3)–Os(3) 57.005(14), Os(2)–Os(3)–Os(1) 60.773(18), Os(3)–S(1)–Os(2) 70.78(7).

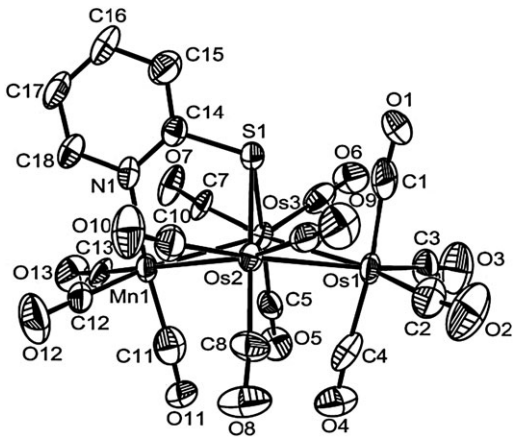

Fig. 2 ORTEP diagram of the molecular structure of $[Os_3Mn(CO)_{13}(\mu_3\text{-pyS})]$ (**4**), showing 50% probability thermal ellipsoids. Ring hydrogen atoms are omitted for clarity. Selected interatomic distances (Å) and angles (°): Os(1)–Os(2) 2.8613(5), Os(1)–Os(3) 2.8600(5), Os(2)–Os(3) 2.7874(4), Os(2)–Mn(1) 2.8147(11), Os(3)–Mn(1) 2.8632(11), Os(2)–S(1) 2.4001(19), Os(3)–S(1) 2.4051(18), Mn(1)–N(1) 2.104(6), C(14)–S(1) 1.769(8), Os(3)–Os(1)–Os(2) 58.313(11), Os(3)–Os(2)–Mn(1) 61.47(2), Os(1)–Os(2)–Mn(1) 118.52(3), Os(2)–Os(3)–Mn(1) 59.73(2), Os(3)–Os(2)–Os(1) 60.820(12), Os(1)–Os(3)–Mn(1) 116.96(3), Os(2)–Mn(1)–Os(3) 58.80(2), Os(2)–Os(3)–Os(1) 60.866(12), Os(2)–S(1)–Os(3) 70.91(5).

and ligand attachments could not be ascertained and thus a single-crystal X-ray diffraction analysis was carried out. An ORTEP diagram of the molecular structure of **7** is shown in Fig. 4 and selected bond distances and angles are listed in the caption. The molecule comprises of two $[Ru_2(CO)_6(\mu\text{-py})]$ units linked by a μ_4-S atom. The twelve carbonyl ligands are equally distributed to all four ruthenium atoms. The bridging

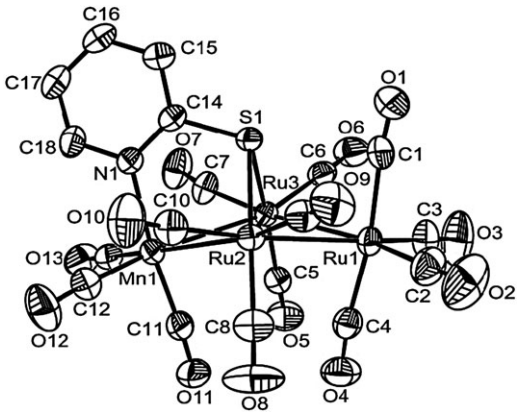

Fig. 3 ORTEP diagram of the molecular structure of $[Ru_3Mn(CO)_{13}(\mu_3\text{-pyS})]$ (**6**), showing 50% probability thermal ellipsoids. Ring hydrogen atoms are omitted for clarity. Selected interatomic distances (Å) and angles (°): Ru(1)–Ru(2) 2.8347(4), Ru(1)–Ru(3) 2.8408(4), Ru(2)–Ru(3) 2.7929(3), Ru(2)–Mn(1) 2.8050(5), Ru(3)–Mn(1) 2.8739(6), Ru(2)–S(1) 2.3761(8), Ru(3)–S(1) 2.3780(8), Mn(1)–N(1) 2.090(3), C(14)–S(1) 1.773(3), Ru(3)–Ru(1)–Ru(2) 58.957(9), Ru(1)–Ru(2)–Mn(1) 118.702(14), Ru(2)–Ru(3)–Mn(1) 59.318(12), Ru(1)–Ru(3)–Mn(1) 116.211(14), Ru(3)–Ru(2)–Ru(1) 60.630(9), Ru(3)–Ru(2)–Mn(1) 61.778(13), Ru(3)–Mn(1)–Ru(2) 58.904(12), Ru(1)–Ru(3)–Ru(2) 60.413(9), Ru(3)–S(1)–Ru(2) 71.96(2).

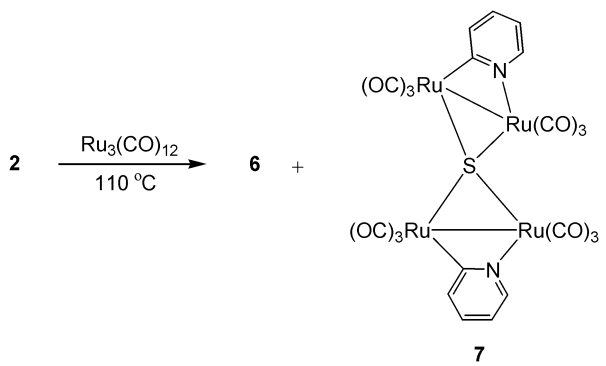

Scheme 3

2-pyridyl ligands, formed by the cleavage of the C–S bond of the pyridine-2-thiolato ligand, spans across two different ruthenium–ruthenium vectors and act as three-electron donors. The nitrogen and carbon atoms of the pyridine ring attached to the metal centers are disordered. The two Ru–Ru bond lengths in **7** are almost equal [Ru(1)–Ru(2) 2.7200(3) Å and Ru(3)–Ru(4) 2.7204(3) Å] and lie in the shorter side of the range reported in literature.[20,23] The coordination geometry of the μ_4-S atoms is severely distorted from tetrahedral geometry. There are two small and four large Ru–S–Ru angles at the μ_4-S atom, and the Ru–S bond distances are similar to those observed in related complexes.[20]

(b) Reactions of $Fe_3(CO)_{12}$ with 1 and 2

Reaction of $[Re_2(CO)_6(\mu\text{-pyS})_2]$ (**1**) with $Fe_3(CO)_{12}$ at 110 °C in toluene (25 min) led to the isolation of the mixed-metal cluster $[Fe_2Re_2(CO)_{13}(\mu\text{-py})](\mu\text{-pyS})(\mu_4\text{-S})]$ (**8**) as red crystals in 20% yield. In contrast, a similar reaction between $[Mn_2(CO)_6(\mu\text{-pyS})_2]$ (**2**) and $Fe_3(CO)_{12}$ did not afford any

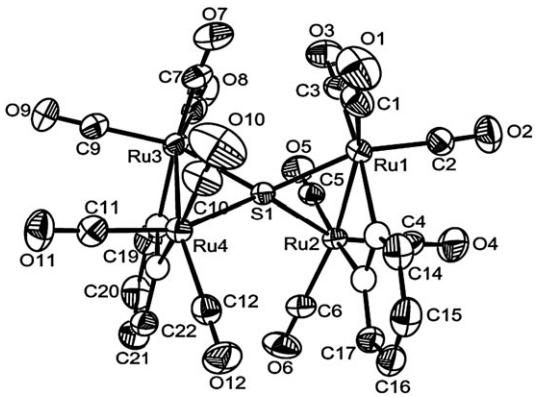

Fig. 4 ORTEP diagram of the molecular structure of $[Ru_4(CO)_{12}(\mu\text{-py})_2(\mu_4\text{-S})]$ (**7**), showing 35% probability thermal ellipsoids. Ring hydrogen atoms are omitted for clarity. Selected interatomic distances (Å) and angles (°): Ru(1)–Ru(2) 2.7200(3), Ru(3)–Ru(4) 2.7204(3), Ru(1)–N(1B) 2.106(2), Ru(4)–N(2A) 2.090(2), Ru(2)–N(1A) 2.109(2), Ru(3)–N(2B) 2.101(2), Ru(1)–S(1) 2.3727(6), Ru(2)–S(1) 2.3722(6), Ru(3)–S(1) 2.3673(6), Ru(4)–S(1) 2.3781(6), Ru(1)–S(1)–Ru(2) 69.954(18), Ru(3)–S(1)–Ru(4) 69.958(17), Ru(2)–S(1)–Ru(4) 134.23(3), Ru(2)–S(1)–Ru(3) 131.37(3), Ru(4)–S(1)–Ru(1) 134.78(3), Ru(3)–S(1)–Ru(1) 128.04(3), N(2B)–Ru(3)–Ru(4) 70.72(6), N(2A)–Ru(4)–Ru(3) 70.89(6), S(1)–Ru(3)–Ru(4) 55.208(15), S(1)–Ru(4)–Ru(3) 54.835(15).

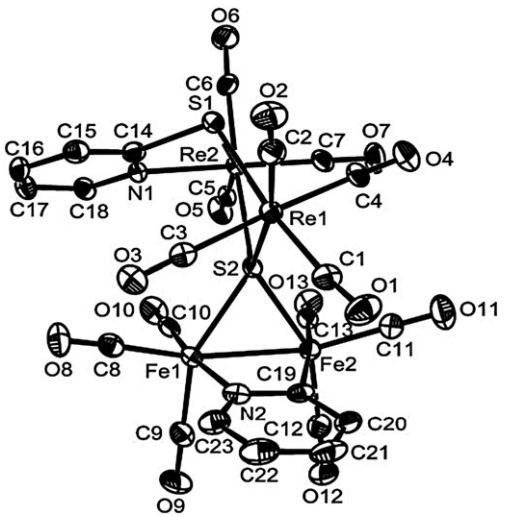

Fig. 5 ORTEP diagram of the molecular structure of $[Fe_2Re_2(CO)_{13}(\mu\text{-py})](\mu\text{-pyS})(\mu_4\text{-S})]$ (**8**), showing 50% probability thermal ellipsoids. Ring hydrogen atoms are omitted for clarity. Selected interatomic distances (Å) and angles (°): Fe(1)–Fe(2) 2.5731(11), Fe(2)–C(19) 1.991(5), Fe(1)–N(2) 1.974(4), Re(2)–N(1) 2.167(4), Fe(2)–S(2) 2.2756(13), Fe(1)–S(2) 2.2921(13), Re(1)–S(1) 2.5021(12), Re(1)–S(2) 2.5527(11), Re(2)–S(1) 2.5450(12), Re(2)–S(2) 2.5569(11), C(10)–Fe(2)–Fe(1) 70.83(15), N(1)–Re(2)–S(1) 65.36(11), N(2)–Fe(1)–Fe(2) 73.01(13), S(2)–Fe(1)–Fe(2) 55.41(4), Fe(2)–S(2)–Fe(1) 68.57(4), Fe(2)–S(2)–Re(2) 123.88(5), Fe(1)–S(2)–Re(2) 124.29(5), Fe(2)–S(2)–Re(1) 123.62(5), Fe(1)–S(2)–Re(1) 121.73(5), Re(1)–S(2)–Re(2) 96.49(4), Re(1)–S(1)–Re(2) 98.09(4).

isolable mixed-metal clusters, leading instead to the tetrairon complex $[Fe_4(CO)_{12}(\mu\text{-py})_2(\mu_4\text{-S})]$ (**9**) in 27% yield (Scheme 4). Both new compounds have been characterized by elemental analysis, IR and ^{1}H NMR spectroscopic data together with single-crystal X-ray diffraction studies.

An ORTEP diagram of the molecular structure of compound **8** is depicted in Fig. 5, and selected bond distances and angles are listed in the caption. The molecule contains $[Fe_2(CO)_6(\mu\text{-py})]$ and $[Re_2(CO)_7(\mu\text{-pyS})]$ fragments linked by a μ_4-S atom. There is only one metal–metal bond within the molecule [Fe(1)–Fe(2) 2.574(2) Å]. The coordination mode of the bridging pyridyl ligand is similar to that observed in **7**, and Fe–C and Fe–N bond distances are within the range reported for related compounds in the literature.[24] The μ-pyS ligand bridges the two non-bonded rhenium atoms and acts as a five-electron donor, nitrogen coordination to the rhenium tricarbonyl unit leading to formation of a four-membered chelate ring. The distortion from the tetrahedral coordination geometry at the μ_4-S atom in **8** is less severe compared to **7** and the Re–S and Fe–S bond distances are in the range found in the literature.[25] The overall structure of compound **8** is very similar to that of $[Re_2Ru_2(CO)_{13}(\mu\text{-py})](\mu\text{-pyS})(\mu_4\text{-S})]$ reported by Deeming *et al*. which crystallizes in two isomeric forms that differ by the orientation of the 2-pyridyl ring within the rhenium fragment. The ^{1}H NMR spectrum of compound **8** displays four doublets and an equal number of triplets (each integrating to 1H), indicating the presence of two non-equivalent 2-pyridyl rings, consistent with the X-ray structure.

An ORTEP diagram of the molecular structure of compound **9** is depicted in Fig. 6, and selected bond distances and angles are listed in the caption. Compound **9** is the iron analogue of **7** and contains two $[Fe_2(CO)_6(\mu\text{-py})]$ units linked by a μ_4-S atom. Like **7**, the coordination geometry at the μ_4-S

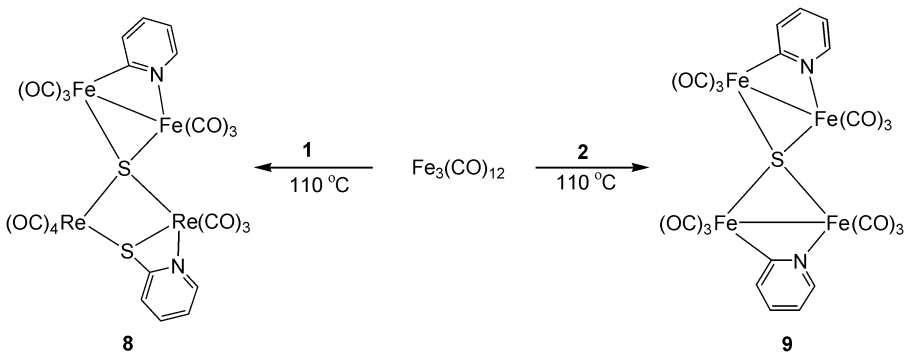

Scheme 4

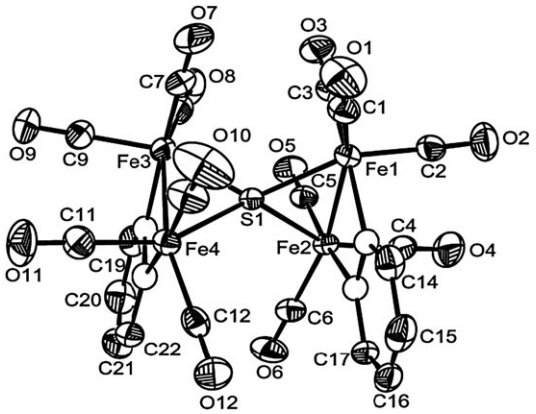

Fig. 6 ORTEP diagram of the molecular structure of $[Fe_4(CO)_{12}(\mu\text{-py})_2(\mu_4\text{-S})]$ (**9**), showing 35% probability thermal ellipsoids. Ring hydrogen atoms are omitted for clarity. Selected interatomic distances (Å) and angles (°): Fe(1)–Fe(2) 2.6015(8), Fe(3)–Fe(4) 2.5965(8), Fe(2)–N(1A) 1.987(3), Fe(3)–N(2B) 1.988(4), Fe(1)–N(1B) 1.982(3), Fe(4)–N(2A) 1.986(3), Fe(1)–S(1) 2.2330(10), Fe(2)–S(1) 2.2505(10), Fe(3)–S(1) 2.2312(10), Fe(4)–S(1) 2.2508(10), Fe(1)–S(1)–Fe(2) 70.93(3), Fe(3)–S(1)–Fe(4) 70.80(3), Fe(2)–S(1)–Fe(4) 131.13(4), Fe(2)–S(1)–Fe(3) 132.28(4), Fe(4)–S(1)–Fe(1) 134.55(4, Fe(3)–S(1)–Fe(1) 128.45(4), N(1B)–Fe(1)–Fe(2) 71.53(11), N(1A)–Fe(2)–Fe(1) 71.73(9), S(1)–Fe(1)–Fe(2) 54.85(3), S(1)–Fe(2)–Fe(1) 54.22(3).

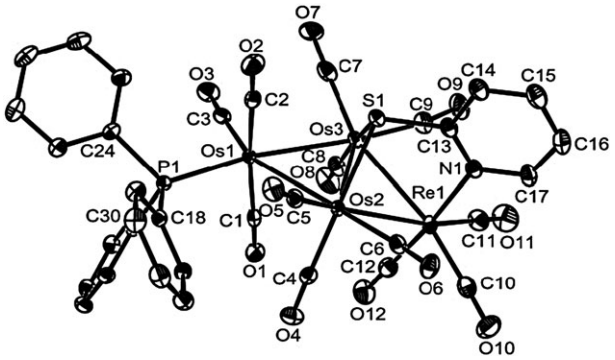

Fig. 7 ORTEP diagram of the molecular structure of $[ReOs_3(CO)_{12}(PPh_3)(\mu_3\text{-pyS})]$ (**10**), showing 50% probability thermal ellipsoids. Ring hydrogen atoms are omitted for clarity. Selected interatomic distances (Å) and angles (°): Os(1)–Os(2) 2.8830(3), Os(1)–Os(3) 2.8633(3), Os(2)–Os(3) 2.7982(2), Os(2)–Re(1) 2.9087(3), Os(3)–Re(1) 2.8955(2), Os(2)–S(1) 2.4060(7), Os(3)–S(1) 2.3956(7), Re(1)–N(1) 2.233(2), Os(1)–P(1) 2.3487(7), C(13)–S(1) 1.776(3), Os(3)–Os(1)–Os(2) 58.281(4), Os(2)–Os(3)–Re(1) 61.416(7), Os(1)–Os(3)–Re(1) 116.289(5), Os(1)–Os(2)–Re(1) 115.248(6), Os(3)–Os(2)–Os(1) 60.508(8), Os(3)–Os(2)–Re(1) 60.940(5), Os(3)–Re(1)–Os(2) 57.644(5), Os(2)–Os(3)–Os(1) 61.211(6), Os(3)–S(1)–Os(2) 71.290(19), C(3)–Os(1)–P(1) 92.79(9), C(1)–Os(1)–P(1) 90.42(8).

atom is severely distorted from the tetrahedral geometry and there are two small and four large Fe–S–Fe angles at the μ_4-S atom. The two iron–iron bond distances in **9** [Fe(1)–Fe(2) 2.6015(8) Å and Fe(3)–Fe(4) 2.5965(8) Å] are quite similar to each other, but are a little bit longer than that of **8** [2.574(2) Å]. The μ-py ligands span across the iron–iron vectors in a similar fashion observed in **7**. The ^{1}H NMR spectrum of **9** displays four equally intense multiplets in the aromatic region while the FAB mass spectrum exhibits a parent molecular ion at m/z 748 and further ions due to stepwise loss of twelve carbonyl groups which is consistent with the X-ray structure.

(c) Reactivity of $[ReOs_3(CO)_{13}(\mu_3\text{-pyS})]$ (3) with PPh_3

The high yield synthesis of **3** promoted us to investigate its reactivity towards phosphines. In the presence of Me_3NO, addition of two equivalents of PPh_3 at 25 °C to a dichloromethane solution of **3** furnishes $[ReOs_3(CO)_{12}(PPh_3)(\mu_3\text{-pyS})]$ (**10**) and $[ReOs_3(CO)_{11}(PPh_3)_2(\mu_3\text{-pyS})]$ (**11**) in 12 and 42% yields, respectively (Scheme 5). The $^{31}P\{^1H\}$ NMR spectrum of **10** displays only a singlet, whereas that of **11** exhibits two singlets, suggesting that they are mono- and bis(phosphine)-substituted derivatives of **3**, respectively. In order to ascertain the exact disposition of the phosphine ligands, X-ray diffraction analyses were carried out for both the compounds, the results of which are depicted in Fig. 7 and Fig. 8.

Both possess the same butterfly core of four metal atoms with the rhenium atom at a wingtip. The pyridine-2-thiolato ligand is located in the same position within the molecule and bonded to the metals in a similar way observed in **3**. In compound **10**, a single PPh_3 ligand occupies an equatorial coordination site on the wingtip osmium. In the bis(phosphine)-substituted **11**, one PPh_3 ligand is bonded to a hinge osmium atom, while the other is equatorially bonded to the wingtip osmium, and they lie *trans* to each other. The Os–P bond distances [2.3487(7) Å in **10**; 2.3584(13) and 2.3847(12) Å in **11**] are within the range found in the literature[26] while the Os–S and Re–N bond distances in both complexes are

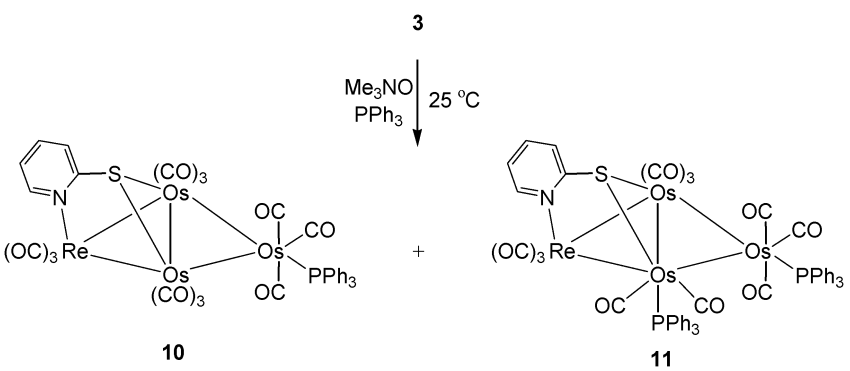

Scheme 5

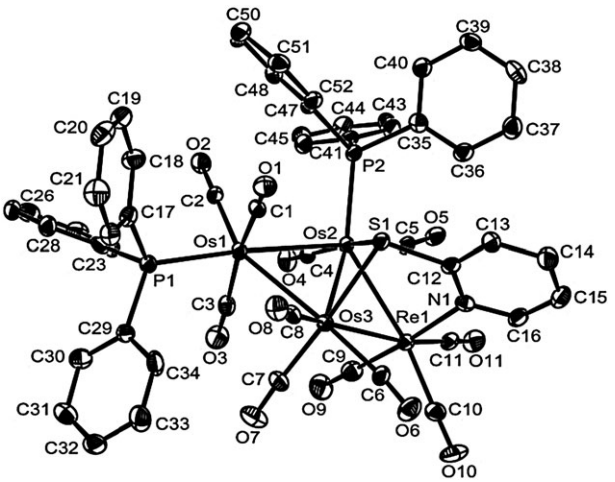

Fig. 8 ORTEP diagram of the molecular structure of $[ReOs_3(CO)_{11}(PPh_3)_2(\mu_3\text{-}pyS)]$ (**11**), showing 50% probability thermal ellipsoids. Ring hydrogen atoms are omitted for clarity. Selected interatomic distances (Å) and angles (°): Os(1)–Os(2) 2.8896(3), Os(1)–Os(3) 2.8833(3), Os(2)–Os(3) 2.7980(3), Os(2)–Re(1) 2.8943(3), Os(3)–Re(1) 2.9320(3), Os(2)–S(1) 2.4060(12), Os(3)–S(1) 2.4113(12), Re(1)–N(1) 2.227(4), Os(1)–P(1) 2.3584(13), Os(2)–P(2) 2.3847(12), C(12)–S(1) 1.771(5), Os(3)–Os(1)–Os(2) 57.982(7), Os(2)–Os(3)–Re(1) 60.624(7), Os(1)–Os(2)–Re(1) 115.991(9), Os(1)–Os(3)–Re(1) 115.008(9), Os(3)–Os(2)–Os(1) 60.895(7), Os(3)–Os(2)–Re(1) 61.978(8), Os(2)–Re(1)–Os(3) 57.397(7), Os(2)–Os(3)–Os(1) 61.123(7), Os(2)–S(1)–Os(3) 71.02(3), C(3)–Os(1)–P(1) 88.56(16), C(2)–Os(1)–P(1) 88.92(16), P(1)–Os(1)–Os(3) 119.03(3), C(4)–Os(2)–P(2) 94.94(16), P(2)–Os(2)–S(1) 92.47(4), P(2)–Os(2)–Os(3) 139.83(3).

comparable to corresponding distances observed in **3**. All other features of the molecules are similar to those of **3**.

Conclusions

Dimeric pyridine-thiolate complexes $[M_2(CO)_6(\mu\text{-}pyS)_2]$ (**1**, M = Re; **2**, M = Mn) act as a useful source for a $M(CO)_3(pyS)$ fragment, reacting with trinuclear group 8 metal carbonyls to afford mixed-metal butterfly clusters $[M'_3M(CO)_{13}(\mu_3\text{-}pyS)]$ in good to moderate yields, behaviour which parallels that reported for $[M_2(CO)_6(\mu\text{-}SN_2C_4H_5)_2]$ (M = Re, Mn). The mixed Os_3M complexes obtained in good yields has facilitated a preliminary exploration of their reactivity; addition of one or two equivalents of PPh_3 to **3** results in carbonyl substitution, while importantly the tetranuclear core was maintained. In future work we aim to further probe this reactivity in order to fully access the conditions under which the cluster core is stable. The selective nature of the substitution suggests that the steric and electronic properties of this cluster type can be easily tailored by judicious choice of phosphine and we aim to exploit this. In contrast, reaction of **1** with $Fe_3(CO)_{12}$ at 110 °C affords the mixed Fe–Re complex $[Fe_2Re_2(CO)_{13}(\mu\text{-}py)(\mu\text{-}pyS)(\mu_4\text{-}S)]$ (**8**), while with **2** the tetrairon cluster $[Fe_4(CO)_{12}(\mu\text{-}py)_2(\mu_4\text{-}S)]$ (**9**) results. The difference in reactivity of the dimers toward $Fe_3(CO)_{12}$ is not unprecedented and is also observed in the case of $[M_2(CO)_6(\mu\text{-}SN_2C_4H_5)_2]$ dimers.[21,22] It probably results from the weaker Fe–Fe *vs*. Ru–Ru or Os–Os bond strength, resulting in iron–iron bond scission presumably to form reactive intermediates which can undergo oxidative addition of one or more carbon–sulfur bonds. It is well-known that carbon–sulfur bond cleavage occurs readily at higher temperatures in the presence of iron carbonyls, and hence the synthesis of iron-containing butterfly clusters of this type requires the development of more labile iron carbonyl precursors – something we are currently investigating.

Experimental section

Unless otherwise noted, all the reactions were carried out under a nitrogen atmosphere using standard Schlenk techniques. Reagent-grade solvents were dried using appropriate drying agents and distilled prior to use by standard methods. Infrared spectra were recorded on a Shimadzu FTIR 8101 spectrophotometer. NMR spectra were recorded on a Bruker DPX 400 instrument. Mass spectra were recorded on a Varian Mat 312 mass spectrometer. Elemental analyses were performed by Microanalytical Laboratories, University College London. Metal carbonyls were purchased from Strem Chemical Inc. and used without further purification. Pyridine-2-thiol was purchased from Aldrich and used as received. The compounds $[Os_3(CO)_{10}(NCMe)_2]$,[25] $[Re_2(CO)_6(\mu\text{-}pyS)_2]$[19] (**1**), and $[Mn_2(CO)_6(\mu\text{-}pyS)_2]$[16f] (**2**) were prepared according to the published procedures.

Reaction of 1 with $[Os_3(CO)_{10}(NCMe)_2]$

A benzene solution (30 mL) of $[Os_3(CO)_{10}(NCMe)_2]$ (250 mg, 0.268 mmol) and **1** (100 mg, 0.131 mmol) was refluxed for 2 h during which time the color of the reaction mixture changed to deep red. The solution was concentrated in *vacuo* and the residue separated by TLC on silica gel. Elution with hexane–acetone (4 : 1, v/v) developed a deep red band which afforded $[ReOs_3(CO)_{13}(\mu_3\text{-}pyS)]$ (**3**) (228 mg, 71%) as red crystals after recrystallization from hexane–CH_2Cl_2 at 25 °C. Spectral data for **3**: Anal. calc. for $C_{18}H_4NO_{13}Os_3ReS$: C, 17.55; H, 0.33; N, 1.13. Found: C, 17.72; H, 0.39; N, 1.21%. IR (ν_{CO}, CH_2Cl_2): 2110 (m), 2043 (vs), 2027 (sh), 2010 (m), 1981 (w), 1962 (m, br), 1918 (w, br) cm^{-1}. ^1H NMR (acetone-d_6): δ 9.78 (d, J = 7.2 Hz, 1H), 8.40 (d, J = 7.2 Hz, 1H), 8.12 (t, J = 7.2 Hz, 1H), 7.60 (t, J = 7.2 Hz, 1H). MS: m/z 1232 (M^+).

Reaction of 2 with $[Os_3(CO)_{10}(NCMe)_2]$

A mixture of $[Os_3(CO)_{10}(NCMe)_2]$ (250 mg, 0.268 mmol) and **2** (65 mg, 0.130 mmol) in benzene (30 mL) was heated to reflux for 2 h during which time the color of the reaction mixture changed from orange to red. The solvent was removed by rotary evaporation and the residue separated by TLC on silica gel. Elution with hexane–acetone (7 : 3, v/v) developed a deep red band which afforded $[MnOs_3(CO)_{13}(\mu_3\text{-}pyS)]$ (**4**) (211 mg, 74%) as deep red crystals after recrystallization from hexane–CH_2Cl_2 at 25 °C. Spectral data for **4**: Anal. calc. for $C_{18}H_4MnNO_{13}Os_3S$: C, 19.65; H, 0.36; N, 1.27. Found: C, 19.83; H, 0.44; N, 1.35%. IR (ν_{CO}, CH_2Cl_2): 2109 (m), 2041 (vs), 2024 (sh), 2000 (m), 1979 (w), 1960 (m, br), 1918 (w, br) cm^{-1}. ^1H NMR (CD_2Cl_2): δ 10.07 (d, J = 6.8 Hz, 1H), 8.10 (d, J = 6.8 Hz, 1H), 7.83 (t, J = 6.8 Hz, 1H), 7.47 (t, J = 6.8 Hz, 1H). MS: m/z 1100 (M^+).

Reaction of 1 with $Ru_3(CO)_{12}$ at 80 °C

A benzene solution (30 mL) of $Ru_3(CO)_{12}$ (200 mg, 0.313 mmol) and **1** (240 mg, 0.315 mmol) was heated to reflux for 2 h. The solvent was removed under reduced pressure and the residue separated by TLC on silica gel. Elution with hexane/acetone (4 : 1, v/v) developed several bands. The major band gave $[ReRu_3(CO)_{13}(\mu_3\text{-pyS})]$ (**5**) (127 mg, 42%) as deep red crystals after recrystallization from hexane–CH_2Cl_2 at 4 °C while the content of the minor bands were too small for complete characterization. Spectral data for **5**: Anal. calc. for $C_{18}H_4NO_{13}ReRu_3S$: C, 22.43; H, 0.42; N, 1.45. Found: C, 22.65; H, 0.51; N, 1.53%. IR (ν_{CO}, CH_2Cl_2): 2102 (m), 2042 (s), 2024 (m), 2011 (m), 1965 (w, br), 1918 (w), 1907 (w) cm^{-1}. ^1H NMR ($CDCl_3$): δ 9.32 (d, J = 6.8 Hz, 1H), 8.26 (d, J = 6.8 Hz, 1H), 7.81 (t, J = 6.8 Hz, 1H), 7.32 (t, J = 6.8 Hz, 1H). MS: m/z 963 (M^+).

Reaction of 2 with $Ru_3(CO)_{12}$ at 80 °C

To a benzene solution (30 mL) of $Ru_3(CO)_{12}$ (260 mg, 0.407 mmol) was added **2** (200 mg, 0.401 mmol) and the mixture was refluxed for 1 h during which time the color of the reaction mixture changed from red to deep red. The solvent was removed under reduced pressure and the residue chromatographed by TLC on silica gel. Elution with hexane–acetone (9 : 1, v/v) developed several bands. The major band gave $[MnRu_3(CO)_{13}(\mu_3\text{-pyS})]$ (**6**) (127 mg, 38%) as deep red crystals after recrystallization from hexane–CH_2Cl_2 at 4 °C while the content of the minor bands were too small for characterization. Spectral data for **6**: Anal. calc. for $C_{18}H_4MnNO_{13}Ru_3S$: C, 25.97; H, 0.48; N, 1.68. Found: C, 26.13; H, 0.55; N, 1.76%. IR (ν_{CO}, hexane): 2102 (m), 2041 (vs), 2024 (m), 1999 (m, br), 1967 (w, br), 1943 (w) cm^{-1}. ^1H NMR ($CDCl_3$): δ 9.15 (d, J = 6.8 Hz, 1H), 8.02 (d, J = 6.8 Hz, 1H), 7.72 (t, J = 6.8 Hz, 1H), 7.29 (t, J = 6.8 Hz, 1H). MS: m/z 832 (M^+).

Reaction of 2 with $Ru_3(CO)_{12}$ at 110 °C

A toluene solution (30 mL) of $Ru_3(CO)_{12}$ (260 mg, 0.407 mmol) and **2** (200 mg, 0.401 mmol) was refluxed for 25 min during which time the color of the reaction mixture changed from red to deep red. The solvent was removed under reduced pressure and the residue chromatographed by TLC on silica gel. Elution with hexane developed several bands. The first and second bands gave the following two compounds in order of elution: $[Ru_4(CO)_{12}(\mu\text{-py})_2(\mu_4\text{-S})]$ (**7**) (123 mg, 43%) as orange crystals and $[MnRu_3(CO)_{13}(\mu_3\text{-pyS})]$ (**6**) (80 mg, 24%) as deep red crystals after recrystallization from hexane–CH_2Cl_2 at 4 °C. Spectral data for **7**: Anal. calc. for $C_{22}H_8N_2O_{12}Ru_4S$: C, 28.46; H, 0.87; N, 3.02. Found: C, 28.62; H, 0.93; N, 3.12%. IR (ν_{CO}, hexane): 2087 (w), 2060 (m), 2049 (s), 2014 (m), 1999 (m, br), 1981 (w) cm^{-1}. ^1H NMR ($CDCl_3$): δ 7.81 (d, J = 6.8 Hz, 2H), 7.57 (d, J = 6.8 Hz, 2H), 7.02 (t, J = 6.8 Hz, 2H), 6.83 (t, J = 6.8 Hz, 2H). MS: m/z 928 (M^+).

Reaction of 1 with $Fe_3(CO)_{12}$

A toluene solution (30 mL) of $Fe_3(CO)_{12}$ (132 mg, 0.262 mmol) and **1** (100 mg, 0.131 mmol) was heated to reflux for 25 min. The solution was concentrated in *vacuo* and the deep red residue subjected to chromatographic separation on silica gel TLC plates. Elution with hexane–acetone (4 : 1, v/v) developed a deep red band which afforded $[Fe_2Re_2(CO)_{13}(\mu\text{-py})](\mu\text{-pyS})(\mu_4\text{-S})]$ (**8**) (28 mg, 20%) as red crystals after recrystallization from hexane–CH_2Cl_2 at 4 °C. Spectral data for **8**: Anal. calc. for $C_{23}H_8Fe_2N_2O_{13}Re_2S_2$: C, 25.85; H, 0.75; N, 2.62. Found: C, 26.01; H, 0.83; N, 2.71%. IR (ν_{CO}, CH_2Cl_2): 2107 (w), 2064 (s), 2031 (vs), 1997 (m), 1985 (m), 1952 (m, br), 1923 (m, br) cm^{-1}. ^1H NMR (CD_2Cl_2): δ 8.48 (d, J = 5.8 Hz, 1H), 8.01 (t, J = 7.6 Hz, 1H), 7.60 (d, J = 5.8 Hz, 1H), 7.57 (t, J = 5.8 Hz, 1H), 7.35 (d, J = 7.6 Hz, 1H), 7.22 (d, J = 7.6 Hz, 1H), 7.07 (t, J = 7.6 Hz, 1H), 6.78 (t, J = 5.8 Hz, 1H). MS: m/z 1068 (M^+).

Reaction of 2 with $Fe_3(CO)_{12}$

$Fe_3(CO)_{12}$ (202 mg, 0.401 mmol) was added to a toluene solution (30 mL) of **2** (100 mg, 0.200 mmol) and the mixture was heated to reflux for 25 min. The solvent was removed under reduced pressure and the residue separated by TLC on silica gel. Elution with hexane–acetone (9 : 1, v/v) developed three bands. The second band afforded $[Fe_4(CO)_{12}(\mu\text{-py})_2(\mu_4\text{-S})]$ (**9**) (60 mg, 27%) as deep red crystals after recrystallization from hexane–CH_2Cl_2 at −20 °C. The first and third bands were too small for characterization. Spectral data for **9**: Anal. calc. for $C_{22}H_8Fe_4N_2O_{12}S$: C, 35.33; H, 1.08; N, 3.74. Found: C, 35.59; H, 1.17; N, 3.86%. IR (ν_{CO}, CH_2Cl_2): 2078 (w), 2054 (s), 2029 (vs), 2000 (w), 1987 (m, br) cm^{-1}. ^1H NMR ($CDCl_3$): δ 7.69 (m, 2H), 7.45 (m, 2H), 7.04 (m, 2H), 6.78 (m, 2H). MS: m/z 748 (M^+).

Reaction of $[ReOs_3(CO)_{13}(\mu_3\text{-pyS})]$ (3) with PPh_3

A CH_2Cl_2 solution (10 mL) of Me_3NO (10 mg, 0.133 mmol) was added drop-wise to a CH_2Cl_2 solution (20 mL) of **3** (75 mg, 0.061 mmol) and PPh_3 (32 mg, 0.122 mmol) and the mixture was stirred at 25 °C for 2 h. The solvent was then removed under reduced pressure, and the residue chromatographed by TLC on silica gel. Elution with hexane–acetone (4 : 1, v/v) developed two bands. The faster moving minor band afforded $[ReOs_3(CO)_{12}(PPh_3)(\mu_3\text{-pyS})]$ (**10**) (11 mg, 12%) as red crystals while the major band gave $[ReOs_3(CO)_{11}(PPh_3)_2(\mu_3\text{-pyS})]$ (**11**) (43 mg, 42%) as red crystals after recrystallization from hexane–CH_2Cl_2 at 4 °C. Spectral data for **10**: Anal. calc. for $C_{35}H_{19}NO_{12}Os_3PReS$: C, 28.68; H, 1.31; N, 0.95. Found: C, 28.84; H, 1.38; N, 1.03%. IR (ν_{CO}, CH_2Cl_2): 2076 (w), 2026 (vs), 2002 (m), 1997 (m), 1943 (m, br), 1912 (w, br) cm^{-1}. ^1H NMR (CD_2Cl_2): δ 9.48 (d, J = 6.0 Hz, 1H), 7.97 (d, J = 6.0 Hz, 1H), 7.73 (t, J = 6.0 Hz, 1H), 7.51 (m, 15H), 7.20 (t, J = 6.0 Hz, 1H). $^{31}P\{^1H\}$ NMR (CD_2Cl_2): δ 8.7 (s). Spectral data for **11**: Anal. calc. for $C_{52}H_{34}NO_{11}Os_3P_2ReS$: C, 36.74; H, 2.02; N, 0.82. Found: C, 36.95; H, 2.10; N, 0.90%. IR (ν_{CO}, CH_2Cl_2): 2054 (w), 2014 (vs), 1979 (s), 1939 (m, br), 1919 (m, br) cm^{-1}. ^1H NMR (CD_2Cl_2): δ 9.48 (m, 1H), 9.42 (m, 1H), 7.85 (m, 1H), 7.68–7.35 (m, 30H), 7.05 (m, 1H). $^{31}P\{^1H\}$ NMR (CD_2Cl_2): δ 21.4 (s, 1P), 18.6 (s, 1P).

Table 1 Crystallographic data and structure refinement for **3**, **4** and **6–11**

Compound	**3**	**4**	**6**	**7**	**8**	**9**	**10**	**11**
Empirical formula	$C_{18}H_4NO_{13}Os_3ReS$	$C_{18}H_4MnNO_{13}Os_3S$	$C_{18}H_4MnNO_{13}Ru_3S$	$C_{22}H_8N_2O_{12}Ru_4S$	$C_{23}H_8Fe_2N_2O_{13}Re_2S_2$	$C_{22}H_8Fe_4N_2O_{12}S$	$C_{35}H_{19}NO_{12}Os_3PReS$	$C_{52}H_{34}NO_{11}Os_3P_2ReS$
FW	1231.08	1099.82	832.43	928.64	1068.53	747.76	1465.34	1699.60
T (K)	150(2)	298(2)	298(2)	150(2)	100(2)	150(2)	100(2)	100(2)
Wavelength (Å)	0.71073	0.71073	0.71073	0.71073	1.54178	0.71073	0.71073	1.54178
Crystal system	Triclinic	Triclinic	Triclinic	Monoclinic	Triclinic	Monoclinic	Monoclinic	Monoclinic
Space group	$P\bar{1}$	$P\bar{1}$	$P\bar{1}$	$P2_1/n$	$P\bar{1}$	$P2_1/n$	$P2_1/c$	$P2_1/c$
a (Å)	8.439(2)	8.4909(3)	8.5181(3)	9.40890(10)	10.4465(1)	9.1790(9)	13.136(1)	13.7860(3)
b (Å)	10.174(2)	10.1166(9)	10.1387(4)	19.4738(2)	15.4234(2)	19.723(2)	15.138(2)	21.2076(4)
c (Å)	15.109(3)	15.157(1)	15.1751(6)	15.7618(10)	18.4256(2)	15.125 (2)	18.663(2)	16.8447(4)
α (°)	70.584(2)	70.739(5)	70.434(3)	90	86.755(1)	90	90	90
β (°)	84.140(3)	83.786(4)	83.813(3)	92.6190(10)	84.108(1)	91.587(8)	98.300(1)	92.363(1)
γ (°)	88.119(3)	88.325(6)	88.009(5)	90	88.237(1)	90	90	90
Volume (Å^3)	1217.1(4)	1221.9(2)	1227.69(8)	2884.97(19)	2947.39(6)	2737.2(5)	3672.3(6)	4920.7(2)
Z	2	2	2	4	4	4	4	4
D_c (Mg m^{-3})	3.359	2.989	2.252	2.138	2.408	1.815	2.650	2.294
μ(Mo-Kα) (mm^{-1})	20.718	16.205	2.464	2.188	25.339	2.218	13.797	20.497
F(000)	1084	984	792	1768	1992	1480	2664	3160
Crystal size (mm)	0.32 × 0.21 × 0.18	0.15 × 0.15 × 0.15	0.20 × 0.20 × 0.18	0.10 × 0.10 × 0.10	0.22 × 0.20 × 0.19	0.25 × 0.23 × 0.22	0.33 × 0.10 × 0.05	0.33 × 0.21 × 0.13
θ range (°)	1.44–28.25	1.43–25.29	2.13–25.16	2.09–29.11	2.87–67.95	1.70–25.17	1.57–32.02	3.21–68.03
Limiting indices	$-11 \le h \ge 11$, $-13 \le k \ge 13$, $-19 \le l \ge 19$	$-10 \le h \ge 0$, $-12 \le k \ge 12$, $-18 \le l \ge 18$	$0 \le h \ge 10$, $-12 \le k \ge 12$, $-18 \le l \ge 18$	$-12 \le h \ge 12$, $-26 \le k \ge 26$, $-21 \le l \ge 21$	$-12 \le h \ge 12$, $-18 \le k \ge 18$, $0 \le l \ge 22$	$-10 \le h \ge 10$, $0 \le k \ge 23$, $0 \le l \ge 18$	$-19 \le h \ge 19$, $0 \le k \ge 22$, $0 \le l \ge 27$	$-16 \le h \ge 16$, $0 \le k \ge 25$, $0 \le l \ge 19$
Reflections collected	13 410	4822	4708	94 388	24 513	5165	60 539	40 725
Independent reflections (R_{int})	5623 (0.0520)	4427 (0.0164)	4386 (0.0688)	7743 (0.0615)	10 065 (0.0283)	4897 (0.0152)	12 142 (0.0315)	8654 (0.0405)
Max. and min. transmission	0.1181 and 0.0578	0.1948 and 0.1948	0.6654 and 0.6386	0.8109 and 0.8109	0.0878 and 0.0729	0.6411 and 0.6070	0.5756 and 0.0923	0.1828 and 0.0566
Data/restraints/parameters	5623/0/274	4427/0/334	4386/0/334	7743/0/360	10065/0/794	4897/0/360	12142/0/487	8654/0/641
Goodness of fit on F^2	1.134	1.048	1.125	1.031	1.095	0.944	1.013	1.020
Final R indices [$I > 2\sigma(I)$]	$R_1 = 0.0467$, $wR_2 = 0.1293$	$R_1 = 0.0267$, $wR_2 = 0.0672$	$R_1 = 0.0270$, $wR_2 = 0.0716$	$R_1 = 0.0285$, $wR_2 = 0.0567$	$R_1 = 0.0275$, $wR_2 = 0.0705$	$R_1 = 0.0354$, $wR_2 = 0.0721$	$R_1 = 0.0195$, $wR_2 = 0.0430$	$R_1 = 0.0266$, $wR_2 = 0.0641$
R indices (all data)	$R_1 = 0.0507$, $wR_2 = 0.1330$	$R_1 = 0.0387$, $wR_2 = 0.0695$	$R_1 = 0.0335$, $wR_2 = 0.0744$	$R_1 = 0.0506$, $wR_2 = 0.0621$	$R_1 = 0.0295$, $wR_2 = 0.0715$	$R_1 = 0.0734$, $wR_2 = 0.0782$	$R_1 = 0.0246$, $wR_2 = 0.0443$	$R_1 = 0.0298$, $wR_2 = 0.0656$
Largest difference in peak and hole (e Å^{-3})	2.977 and −3.554	1.087 and −1.417	0.549 and −1.170	0.385 and −0.641	1.298 and −0.993	0.347 and −0.331	1.619 and −0.821	1.421 and −0.817

X-ray crystallography

Single crystals were mounted on fibres and diffraction data collected at low temperature (see Table 1) on Bruker SMART APEX (for **3**), Enraf Nonius CAD-4 (for **4**, **6**), Bruker Nonius Kappa CCD (for **7**, **9**) and Bruker APEX2 CCD (for **8**, **10**, **11**) diffractometers using Mo-Kα radiation (λ = 0.71073 Å). Data collection, indexing and initial cell refinements were all done using SMART[27] software. Data reduction was accomplished with SAINT[28] software and the DIFABS[29] and SADABS[30] programs were used to apply empirical absorption corrections. The structures were solved by direct methods[31] and refined by full-matrix least-squares.[32] All non-hydrogen atoms were refined anisotropically and hydrogen atoms were included using a riding model. Scattering factors were taken from International Tables for X-ray Crystallography.[33] Additional details of data collection and structure refinement are given in Table 1.

Acknowledgements

This research has been sponsored by the Ministry of Science and Information & Communication Technology, Government of the People's Republic of Bangladesh.

References

1 (*a*) *Catalysis by Di- and Polynuclear Metal Cluster Complexes*, ed. R. D. Adams and F. A. Cotton, Wiley-VCH, New York, 1998; (*b*) P. Braunstein and J. Rosé, in *Metal Clusters in Catalysis*, ed. P. Braunstein, L. A. Oro and P. R. Raithby, Wiley-VCH, Weinheim, Germany, 1999, vol. 2, pp. 616.

2 (*a*) R. D. Adams, in *Comprehensive Organometallic Chemistry II*, ed. E. W. Abel, F. G. A. Stone and G. Wilkinson, Elsevier, Oxford, 1995, vol. 10, pp. 1; (*b*) P. Braunstein and J. Rosé, in *Comprehensive Organometallic Chemistry II*, ed. E. W. Abel, F. G. A. Stone and G. Wilkinson, Elsevier, Oxford, 1995, vol. 10, pp. 351; (*c*) Y. Chi and D. K. Hwang, in *Comprehensive Organometallic Chemistry II*, ed. E. W. Abel, F. G. A. Stone and G. Wilkinson, Elsevier, Oxford, 1995, vol. 10, pp. 85.

3 (*a*) P. Mathur, A. K. Bhunia, S. M. Mobin, V. K. Singh and C. Srinivasu, *Organometallics*, 2004, **23**, 3694; (*b*) J. N. L. Dennett, S. A. R. Knox, K. M. Anderson, J. P. H. Charmant and A. G. Orpen, *Dalton Trans*., 2005, 63.

4 (*a*) R. D. Adams, B. Captain and M. D. Smith, *Angew. Chem., Int. Ed*., 2006, **45**, 1109; (*b*) R. D. Adams, B. Captain and L. Zhu, *Inorg. Chem*., 2006, **45**, 430.

5 (*a*) L. Quebatte, R. Scopelliti and K. Severin, *Angew. Chem., Int. Ed*., 2004, **43**, 1520; (*b*) N. T. Lucas, J. P. Blitz, S. Petrie, R. Stranger, M. G. Humphrey, G. A. Heath and V. Otieno-Alego, *J. Am. Chem. Soc*., 2002, **124**, 5139; (*c*) A. J. Bridgeman, M. J. Mays and A. D. Woods, *Organometallics*, 2001, **20**, 2932; (*d*) S. Gauthier, R. Scopelliti and K. Severin, *Organometallics*, 2004, **23**, 3769.

6 (*a*) Y. Ishii and M. Hidai, *Catal. Today*, 2001, **66**, 53; (*b*) T. Tanase and R. A. Begum, *Organometallics*, 2001, **20**, 106; (*c*) M. M. Dell'Anna, S. J. Trepanier, R. McDonald and M. Cowie, *Organometallics*, 2001, **20**, 88.

7 (*a*) J. Xiao and R. J. Puddephatt, *Coord. Chem. Rev*., 1995, **143**, 457; (*b*) A. M. Trzeciak and J. J. Ziolkowski, *Coord. Chem. Rev*., 1999, **190–192**, 883.

8 (*a*) R. D. Adams and T. S. Barnard, *Organometallics*, 1998, **17**, 2885; (*b*) R. D. Adams and T. S. Barnard, *Organometallics*, 1998, **17**, 2567; (*c*) R. D. Adams, T. S. Barnard, Z. Li, W. Wu and J. H. Yamamato, *J. Am. Chem. Soc*., 1994, **116**, 9103.

9 (*a*) P. Mathur, A. K. Das, M. Hossain, C. V. V. Satyanarayana, A. L. Rheingold, L. M. Liable-Sands and G. P. A. Yap, *J. Organomet. Chem*., 1997, **532**, 189; (*b*) E. G. Tulsky and J. R. Long, *Inorg. Chem*., 2001, **40**, 6990.

10 (*a*) T. Shima and H. Suzuki, *Organometallics*, 2000, **19**, 2420; (*b*) N. Tsukada, O. Tamura and Y. Inoue, *Organometallics*, 2002, **21**, 2521.

11 (*a*) A. Inagaki, T. Takemori, M. Tanaka and H. Suzuki, *Angew. Chem., Int. Ed*., 2000, **39**, 404; (*b*) Y. Ohki and H. Suzuki, *Angew. Chem., Int. Ed*., 2000, **39**, 3120; (*c*) T. Takemori, A. Inagaki and H. Suzuki, *J. Am. Chem. Soc*., 2001, **123**, 1762.

12 (*a*) Y. Yuan, M. V. Jiménez, E. Sola, F. J. Lahoz and L. A. Oro, *J. Am. Chem. Soc*., 2002, **124**, 752; (*b*) E. K. van den Beuken and B. L. Feringa, *Tetrahedron*, 1998, **54**, 12985; (*c*) P. Kalck, *Polyhedron*, 1988, **7**, 2441.

13 (*a*) J. Knight and M. J. Mays, *J. Chem. Soc., Dalton Trans*., 1972, 1022; (*b*) M. S. Corraine and J. D. Atwood, *Organometallics*, 1991, **10**, 2647.

14 (*a*) R. B. King, *Prog. Inorg. Chem*., 1972, **15**, 237; (*b*) P. Chini, *Inorg. Chim. Acta Rev*., 1968, **2**, 31.

15 (*a*) S. G. Rosenfield, S. A. Swedberg, S. K. Arora and P. K. Mascharak, *Inorg. Chem*., 1986, **25**, 2109; (*b*) A. J. Deeming, K. I. Hardcastle, M. N. Meah, P. A. Bates, H. M. Dawes and M. B. Hursthouse, *J. Chem. Soc., Dalton Trans*., 1988, 227; (*c*) A. J. Deeming, M. Karim and M. Powell, *J. Chem. Soc., Dalton Trans*., 1990, 2321; (*d*) D. J. Rose, Y.-D. Chang, Q. Chen and J. Zubieta, *Inorg. Chem*., 1994, **33**, 5167; (*e*) S. Kitagawa, M. Munakata, H. Shimono, S. Matsuyama and S. Masuda, *J. Chem. Soc., Dalton Trans*., 1990, 2105.

16 (*a*) I. P. Evans and G. Wilkinson, *J. Chem. Soc., Dalton Trans*., 1974, 946; (*b*) B. P. Kennedy and A. B. P. Lever, *Can. J. Chem*., 1972, **50**, 3488; (*c*) K. Umakoshi, A. Ichimura, I. Kinoshita and S. Ooi, *Inorg. Chem*., 1990, **29**, 4005; (*d*) P. Mura, B. J. Olby and S. D. Robinson, *J. Chem. Soc., Dalton Trans*., 1985, 2101; (*e*) B. K. Santra, M. Menon, C. K. Pal and G. K. Lahiri, *J. Chem. Soc., Dalton Trans*., 1997, 1387; (*f*) S. E. Kabir, M. M. Karim, K. Kundu, S. M. B. Ullah and K. I. Hardcastle, *J. Organomet. Chem*., 1996, **517**, 155; (*g*) M. Islam, C. A. Johns, S. E. Kabir, K. Kundu, K. M. A. Malik and S. M. B. Ullah, *J. Chem. Crystallogr*., 1999, **29**, 1001.

17 (*a*) S. G. Rosenfield, H. P. Berends, L. Gelmini, D. W. Stephan and P. K. Mascharak, *Inorg. Chem*., 1987, **26**, 2792; (*b*) R. Castro, M. L. Durán, J. A. Garcia-Vázquez, J. Romero, A. Sousa, A. Castiñeiras, W. Hiller and J. Strähle, *J. Chem. Soc., Dalton Trans*., 1990, 531; (*c*) C. O. Kienitz, C. Thöne and P. Jones, *Inorg. Chem*., 1996, **35**, 3990.

18 (*a*) M. Berardini and J. Brennan, *Inorg. Chem*., 1995, **34**, 6179; (*b*) D. J. Rose, Y.-D. Chang, Q. Chen, P. B. Kettler and J. Zubieta, *Inorg. Chem*., 1995, **34**, 3973; (*c*) Y. Cheng, T. J. Emge and J. G. Brennan, *Inorg. Chem*., 1996, **35**, 342; (*d*) J. Lee, T. J. Emge and J. G. Brennan, *Inorg. Chem*., 1997, **36**, 5064.

19 A. J. Deeming, M. Karim, P. A. Bates and M. B. Hursthouse, *Polyhedron*, 1988, **7**, 1401.

20 (*a*) A. J. Deeming, M. Karim, N. I. Powell and K. I. Hardcastle, *Polyhedron*, 1990, **9**, 623; (*b*) B. Cockerton, A. J. Deeming, M. Karim and K. I. Hardcastle, *J. Chem. Soc., Dalton Trans*., 1991, 431.

21 S. Ghosh, S. E. Kabir, S. Pervin, G. M. G. Hossain, D. T. Haworth, S. V. Lindeman, T. A. Siddiquee, D. W. Bennett and H. W. Roesky, *Z. Anorg. Allg. Chem*., 2009, **635**, 76.

22 S. Ghosh, S. E. Kabir, S. Pervin, A. K. Raha, G. M. G. Hossain, D. T. Haworth, S. V. Lindeman, D. W. Bennett, T. A. Siddiquee, L. Salassa and H. W. Roesky, *Dalton Trans*., 2009, 3510.

23 (*a*) A. W. Coleman, D. F. Jones, P. H. Dixneuf, C. Brisson, J. J. Bonnet and G. Lavigne, *Inorg. Chem*., 1984, **23**, 952; (*b*) N. Lugan, J. J. Bonnet and J. A. Ibers, *J. Am. Chem. Soc*., 1985, **107**, 4484; (*c*) M. I. Bruce, P. A. Humphrey, B. W. Skelton, A. H. White and M. L. Williams, *Aust. J. Chem*., 1985, **38**, 1301; (*d*) M. I. Bruce, O. Bin Shawkataly and M. L. Williams, *J. Organomet. Chem*., 1985, **287**, 127; (*e*) S. E. Kabir, M. R. Hassan, D. T. Haworth, S. V. Lindeman, T. A. Siddiquee and D. W. Bennett, *J. Organomet. Chem*., 2007, **692**, 3936; (*f*) M. I. Bruce, J. R. Hinchliffe, R. Surynt, B. W. Skelton and A. H. White, *J. Organomet. Chem*., 1994, **469**, 89; (*g*) S. E. Kabir and G. Hogarth, *Coord. Chem. Rev*., 2009, **253**, 1285.

24 (*a*) W.-F. Liaw, C.-H. Chen, G.-H. Lee and S.-M. Peng, *Organometallics*, 1998, **17**, 2370; (*b*) N. Choi, G. Conole, M. Kessler, J. D. King, M. J. Mays, M. McPartlin, G. E. Pateman and G. A. Solan, *J. Chem. Soc., Dalton Trans*., 1999, 3941.

25 B. F. G. Johnson, J. Lewis and D. A. Pippard, *J. Chem. Soc., Dalton Trans*., 1981, 407.
26 (*a*) M. I. Bruce, M. J. Liddell, C. A. Hughes, J. M. Patrick, B. W. Skelton and A. H. White, *J. Organomet. Chem*., 1988, **347**, 157; (*b*) W. K. Leong and Y. Liu, *J. Organomet. Chem*., 1999, **584**, 174; (*c*) M. I. Bruce, M. J. Liddell, C. A. Hughes, B. W. Skelton and A. H. White, *J. Organomet. Chem*., 1988, **347**, 181; (*d*) M. A. Mottalib, S. E. Kabir, D.A. Tocher, A. J. Deeming and E. Nordlander, *J. Organomet. Chem*., 2007, **692**, 5007.
27 *SMART Version 5.628*, Bruker AXS, Inc., Madison, WI, 2003.
28 *SAINT Version 6.36*, Bruker AXS, Inc., Madison, WI, 2002.
29 N. Walker and D. Stuart, *Acta Crystallogr., Sect. A: Found. Crystallogr*., 1983, **39**, 158.
30 G. Sheldrick, *SADABS Version 2.10*, University of Göttingen, 2003.
31 *Program XS from SHELXTL package, V. 6.12*, Bruker AXS Inc., Madison, WI, 2001.
32 *Program XL from SHELXTL package, V. 6.12*, Bruker AXS, Inc., Madison, WI, 2001.
33 *International Tables for X-ray Crystallography, Volume C*, ed. A. J. C. Wilson, Kynoch, Academic Publishers, Dordrecht, 1992; Tables 6.1.1.4 (pp. 500–502) and 4.2.6.8 (pp. 219–222).

